Nonlinear Dyn (2025) 113:19541–19557
https://doi.org/10.1007/s11071-025-11171-7

RESEARCH

A statistical sparse jump model for automatic identification of dynamical transitions in the co-orbital regime

Federico P. Cortese · Sara Di Ruzza · Elisa Maria Alessi

Received: 18 December 2024 / Accepted: 26 March 2025 / Published online: 25 April 2025

Abstract Co-orbital dynamics appears in the three-body problem and is widely studied to analyze asteroidal behaviors, but also to design trajectories for interplanetary missions. It involves complex transitions that can be challenging to analyze manually in case of large and lengthy dataset, typically of planetary science, but also in case of parametric analysis that involves different perturbations. For this reason, in this work we employ the statistical sparse jump model, an efficient and robust machine learning model, to classify co-orbital regimes and identify their transitions. The ability of the model to estimate regime-specific parameters and ensure regime persistence provides a significant advantage in capturing the dynamics of these motions. Unlike black-box methods, this model offers interpretable results directly linked to the physical parameters of celestial mechanics. Our method achieves high accuracy in simpler cases and strong performance in more complex scenarios, even with large datasets. Applications to data corresponding to real and simulated trajectories reveal critical insights into the co-orbital dynamics, such as the average duration of regimes and the role of key orbital parameters. This work marks the first application of statistical sparse jump models in orbital dynamics, and contributes to bridge machine learning with celestial mechanics.

Keywords Co-orbital motion · Mean motion resonance · Dynamical transition · Machine learning · Time series analysis · Unsupervised learning

1 Introduction

In celestial mechanics, a co-orbital motion arises in the context of the three-body problem and it occurs when two bodies orbit another one in the same amount of time, on average.

Taking as reference example a system composed by Sun, Earth and an asteroid, the asteroid is in co-orbital motion with the Earth if it performs on average one orbit around the Sun in one year, that is the orbital period of the Earth. In other words, on average, the motion of the asteroid and the one of the Earth are in 1:1 mean motion resonance.

The importance of this dynamics lies in its associated stability. As a matter of fact, in the solar system there have been observed several natural bodies, both asteroids and moons, that follow these configurations for more than hundreds of thousands of years, even if subject to various orbital perturbations. In

F. P. Cortese (✉) · E. M. Alessi
Istituto di Matematica Applicata e Tecnologie Informatiche 'E. Magenes', Consiglio Nazionale delle Ricerche, Via Alfonso Corti 12, 20133 Milan, Italy
e-mail: federico.cortese@mi.imati.cnr.it

E. M. Alessi
e-mail: elisamaria.alessi@cnr.it

S. Di Ruzza
Dipartimento di Matematica e Informatica, Università di Palermo, Via Archirafi 34, 90123 Palermo, Italy
e-mail: sara.diruzza@unipa.it

the field of space engineering, different missions have been proposed to follow, as nominal orbital, a quasi-satellite orbit [18,23,37,49] or to exploit the equilateral Lagrange points of the Sun-Earth system (e.g., [1]), in view of their stable feature and thus low station-keeping costs. There also exist missions aimed to take scientific observations at objects in co-orbital state [35,50].

The examples just mentioned refer to different configurations that can appear in the co-orbital motion, being the main difference the relative phase with respect to the Earth (keeping the Sun-Earth system as reference). They will be specified in detail in the following section. Although they are in general stable, there exists the possibility, well observed in nature (e.g., [16]), that the particle[1] moves from one co-orbital regime to another one. To be able to master these transitions is important because different regimes have different features, that can help to understand the natural evolution of small bodies in the solar system, but that can also be exploited for mission analysis. The works [17,36] have developed a semi-analytical map to classify the co-orbital regimes in the quasi-planar approximation, assuming the Circular Restricted Three-Body Problem (CR3BP). Here, we aim at leveraging artificial intelligence methods for the automatic identification of the co-orbital motions, together with the mutual transitions, when they exist. To make an example, given one or more time series describing the orbital evolution of a particle, the method presented in this work aims at classifying the specific co-orbital configuration and whether, and in case how, it changes over time. This tool is useful to validate the framework where the semi-analytical map can be applied and also to analyze large set of long numerical samples, typical of statistical studies in planetary science (e.g., [21,26]).

In the literature, some studies focus on identifying specific resonant regimes (e.g., [6,8,9,24,45,47]) also with machine learning methods, the latter being particularly promising, but still in its emerging phase [7]. Concerning the identification of dynamical transitions within the 1:1 mean motion resonance, it is usually tackled focusing on single objects (e.g., [5,15]) by visual inspection.

A good method for co-orbital regime identification should determine the time intervals during which a specific orbital regime occurs, characterize the nature of the possible transitions, and accurately account for their persistence, which often lasts for extended periods. This allows for more accurate estimates of transition frequencies, whether certain directions are privileged, and an assessment of whether certain asteroid families exhibit greater stability within specific co-orbital regimes for a given planet-Sun system. Furthermore, an effective method must handle the additional complexity arising from the potential non-resonant dynamical evolution of the particle.

In view of these challenges, we combine celestial mechanics knowledge with advanced machine learning techniques to investigate complex co-orbital motion dynamics in the Sun-Earth system. A review on the state-of-art concerning machine learning applications to celestial mechanics and dynamical astronomy is given in [7,9].

Here, we employ the statistical *sparse jump model* (SJM), an unsupervised learning method introduced in [33] as an alternative to hidden Markov models [3,52]. SJMs belong to the broader class of *regime-switching models*, which are statistical methods designed to identify and analyze systems that switch between distinct states or regimes. In this framework, the dynamics of a given system is assumed to be driven by an unobserved discrete latent process. This process is typically modeled as a Markov chain [31], with each of its states representing a distinct regime. Expanding on this foundation, the authors in [4] introduced statistical *jump models*, a more general framework for capturing regime dynamics. Building further, the authors in [34] extended this approach by incorporating k-means clustering to define localized submodels, enabling the simultaneous identification of regimes and estimation of their parameters. In this context, statistical SJMs [33] enhance the basic regime-switching framework by effectively modeling the persistence of latent regimes and incorporating feature importance analysis: this means that SJMs can identify which variables are most relevant for differentiating between regimes, providing insights into the underlying dynamics. This makes SJM a robust tool for modeling systems characterized by sudden changes and numerous features. The estimation procedure is also fast and efficient, with the key advantage of producing easily interpretable results, as the characteristics of each regime can be directly inferred from the estimated parameters. For example, in our context, regimes correspond to different co-orbital configurations, and their transitions reveal the dynamical processes governing the system. This stands in contrast

[1] In general, a particle can be an asteroid or a spacecraft.

to black-box methods, such as artificial neural networks [51], which may achieve high classification accuracy but often lack interpretability.

SJMs have found applications across a wide range of domains. In finance, they have been employed to study cryptocurrency [11], and equity markets [2,10], for risk management purposes [42], and investment strategies [43]. Beyond finance, these models have also been utilized for air quality assessment [14] and urban thermal comfort monitoring [13].

As far as we know, this is the first time that SJMs are applied to the field of orbital dynamics. Here, the definition of the features is given by theoretical arguments of celestial mechanics. Our results demonstrate perfect classification accuracy in simple cases and strong performance in more complex scenarios. The statistical findings align well with physical principles, offering straightforward result interpretation and valuable insights for future research on the key factors influencing co-orbital regime transitions.

The paper is organized as follows. Section 2 introduces the basic concepts needed to understand the co-orbital motion. Section 3 details the methods used to acquire the data for analysis. Section 4 shows the application of the SJM to the data corresponding to orbits of asteroids that can enter in co-orbital motion with the Earth, proving its effectiveness in identifying the correct regime. Moreover, it highlights the model's strong potential for handling highly complex scenarios where labeling is unfeasible. Section 5 draws some conclusions.

2 The co-orbital motion

In general, an orbit of a celestial body is a conic section, defined by five orbital elements, that describe its size, shape and orientation with respect to a given inertial reference system, namely, *semi-major axis* a, *eccentricity* e, *inclination* i, *longitude of the ascending node* Ω, *argument of pericenter* ω. (See Fig. 1). The position of the particle on the orbit is given by an angular variable, that can be the *mean anomaly* M (the one used in this work), or the true anomaly ν, or the eccentric anomaly E. If the particle[2] is subject only to the gravitational attraction of one massive body (two-body problem), then the orbital elements (except the mean anomaly) would remain constant in time. When a second massive body is added to the system, the orbital elements vary with time. The so-called third-body perturbation can be modeled by the following disturbing function $\mathcal{R}$ [27,41]

$$\mathcal{R} = Gm_P \left(\frac{1}{|\boldsymbol{r} - \boldsymbol{r_P}|} - \frac{\boldsymbol{r} \cdot \boldsymbol{r_P}}{r_P^3} \right), \tag{1}$$

where G is the gravitational constant, m_P is the mass of the second body (the planet) and $\boldsymbol{r}$, $\boldsymbol{r_P}$ are, respectively, the heliocentric positions of the asteroid and the planet (see Fig. 2)[3]. Notice that $\boldsymbol{r}$ and $\boldsymbol{r_P}$ are functions of the corresponding orbital elements, say, $a, e, i, \Omega, \omega, M$ and $a_P, e_P, i_P, \Omega_P, \omega_P, M_P$, respectively.

In general, to obtain the long-term evolution of the orbital elements of the asteroid due to the perturbation, the disturbing function is averaged over the fast variable of the system (for instance, the mean anomaly of the planet [27]). The corresponding function

$$R = Gm_P \left\langle \frac{1}{|\boldsymbol{r} - \boldsymbol{r_P}|} - \frac{\boldsymbol{r} \cdot \boldsymbol{r_P}}{r_P^3} \right\rangle, \tag{2}$$

where $\left\langle \cdot \right\rangle$ stands for the average with respect to a fast variable, depends on the relative orbital elements between the asteroid and the planet, say, $a_r, e_r, i_r, \Omega_r, \omega_r$, where

$$\begin{aligned} a_r &= a - a_P \,, \\ e_r &= \sqrt{e^2 + e_P^2 - 2\, e\, e_P \cos \bar{\omega}_r} \,, \\ i_r &= \sqrt{i^2 + i_P^2 - 2\, i\, i_P \cos \Omega_r} \,, \\ \Omega_r &= \Omega - \Omega_P \,, \\ \omega_r &= \omega - \omega_P \,, \\ \bar{\omega}_r &= \omega_r + \Omega_r \,. \end{aligned} \tag{3}$$

The co-orbital regime occurs when a_r oscillates around 0. When this happens, the asteroid is in a 1:1 mean motion resonance with the planet and the range of oscillation of the *resonant angle*, namely

$$\theta = (M + \Omega + \omega) - (M_p + \Omega_P + \omega_P), \tag{4}$$

[2] Since we focus on the motion of real asteroids or on data coming from numerical simulations on asteroidal motion, in the following we call the particle either the asteroid or the particle, while the secondary be the Earth and the primary the Sun. The reference plane is always the ecliptic.

[3] The disturbing function is obtained by considering the gravitational accelerations of the two massive bodies on the particle and the gravitational acceleration between them. Thus it contains one direct term (the first one), that represents the acceleration of the third body on the particle and one non-direct term (the second one), that represents the fact that the two primaries attract each other.

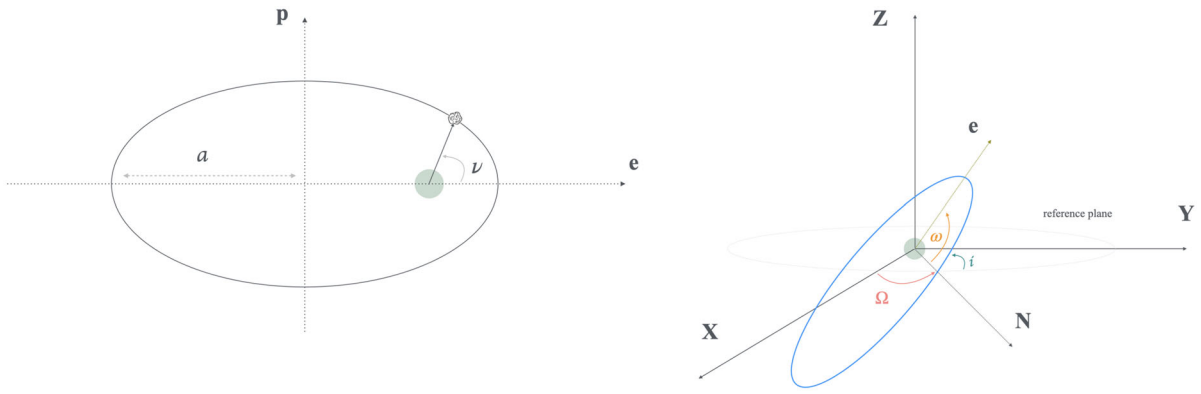

Fig. 1 Definition of orbital elements for an elliptical orbit (left: on the orbital plane, right: three-dimensional representation)

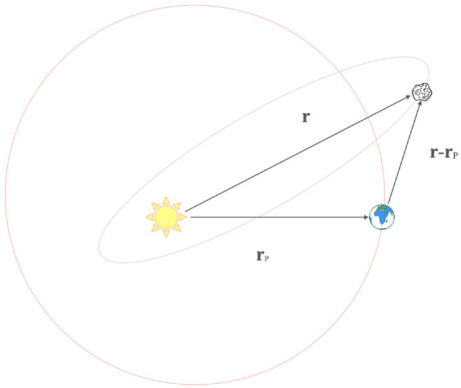

Fig. 2 The geometry of the third-body perturbation

determines the kind of co-orbital regime. The resonant angle is the relative phase between the position of the planet in its orbit around the Sun and the position of the particle in its orbit around the Sun.

In particular, we focus on the following co-orbital regimes (see Fig. 3):

- Tadpole (TP): the relative phase θ oscillates around $\pi/3$ or $5\pi/3$ rad (or $-\pi/3$);
- Horseshoe (HS): the relative phase θ oscillates around π rad;
- Quasi-Satellite (QS): the relative phase θ oscillates around 0 rad.

The same orbits can be seen also in the context of the Circular Restricted Three-Body Problem, assuming that the eccentricity of the orbit of the planet is small enough. We recall that the CR3BP models the motion of a massless particle subject to the simultaneous and comparable gravitational attraction of two massive bodies, that orbit on a circular orbit around their common center of mass [46]. Usually one of the two masses is much larger than the other and thus the barycenter lies within the actual radius of the primary (that is however assumed as a point mass). The motion of the particle is described in a synodic reference system, so that the primaries are fixed on the x-axis. In this reference system, the tadpole, horseshoe and quasi-satellite motion can be visualized as shown in Fig. 4. In the context of the CR3BP, the Earth revolves in a circular Keplerian orbit, that is a reasonable approximation. Thus the relative orbital elements e_r and ω_r are replaced, respectively, by the asteroid orbital elements e and ω.

When the inclination of the orbit of the asteroid is not zero, the asteroid can move within the co-orbital motion between different regimes. This is what we call a *transition* (see Fig. 5, left and right). A transition can occur for two reasons: if the system can be well approximated within the three-body model, then the transition is due to a secular variation in eccentricity and argument of pericenter [28], otherwise the transition is due to an external effect, that is comparable to the gravitational influence of the planet and the Sun on the asteroid.

Apart from transitions involving HS, QS and TP motions, we deal with

- Compound motion (CP): this is a composition of the HS and the QS regimes and it is characterized by the fact that the relative phase oscillates around π, but it crosses the value $\theta = 0$, that does not happen for the HS motion. See Fig. 5 in the middle.

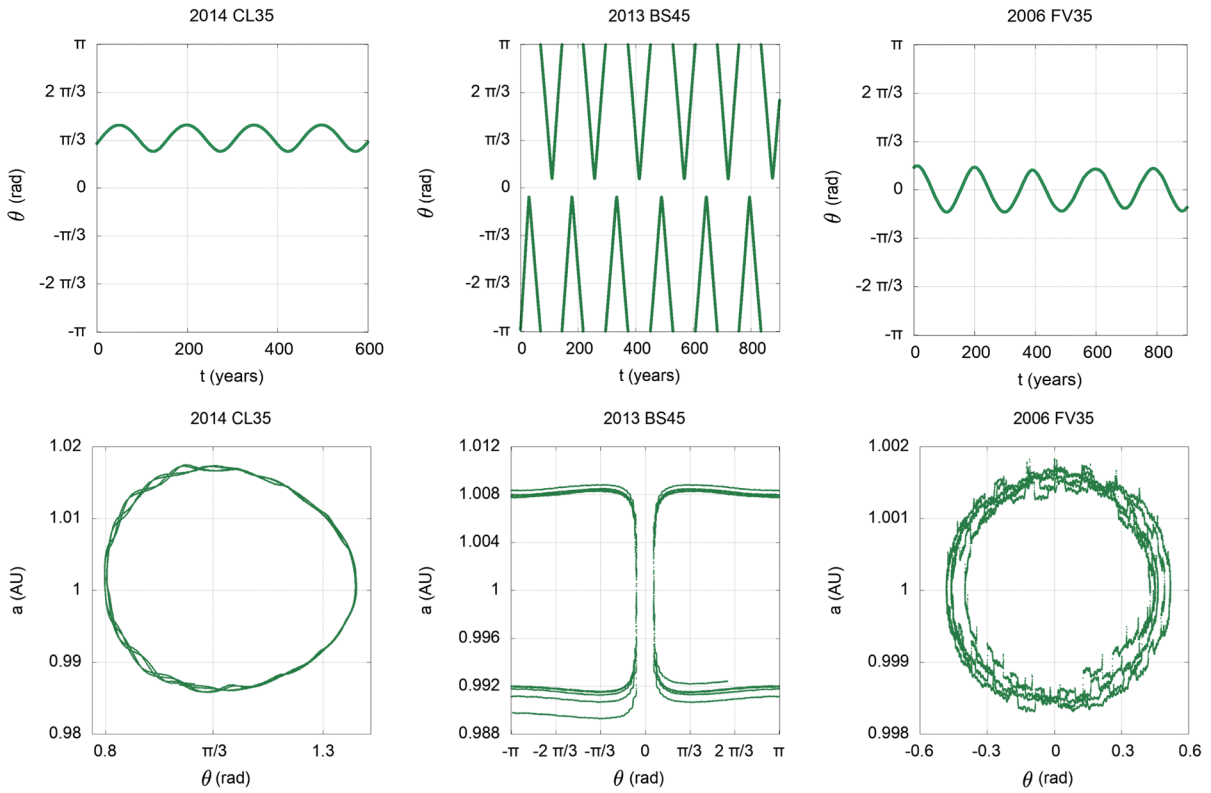

Fig. 3 Co-orbital regimes. Left: tadpole; middle: horseshoe; right: quasi-satellite. In the upper panels the evolution of the resonant angle θ versus time t is plotted and in the lower panels the semi-major axis a versus θ is represented for three real asteroids (the first is a co-orbital of Jupiter and the semi-major axis is scaled to assume that the semi-major axis of Jupiter is 1, the others are co-orbitals of the Earth)

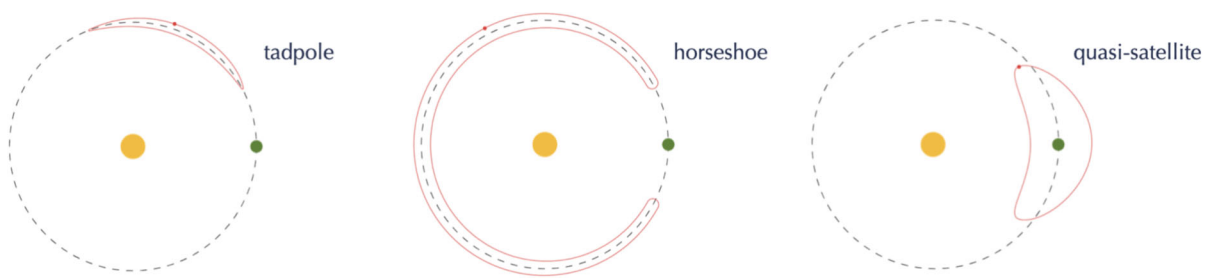

Fig. 4 The classical co-orbital motions in the synodic reference system (in red), the planet (in green), and the Sun (in yellow). The grey dashed line highlights the fact that the co-orbital regimes take place at the same distance with respect to the Sun as the one of the given planet

- Non-resonant (NR) regime: the asteroid is not in mean motion resonance with the planet, that is, the semi-major axis does not oscillate around the mean value of semi-major axis of the planet. In what follows, we consider only Sun-Earth system, and thus NR is characterized by the fact that a does not cross the value $a = 1$ AU.

In Fig. 5, we plot the evolution of the resonant angle θ for three different co-orbital asteroids of the Earth. On the left panels, an asteroid experiencing transitions

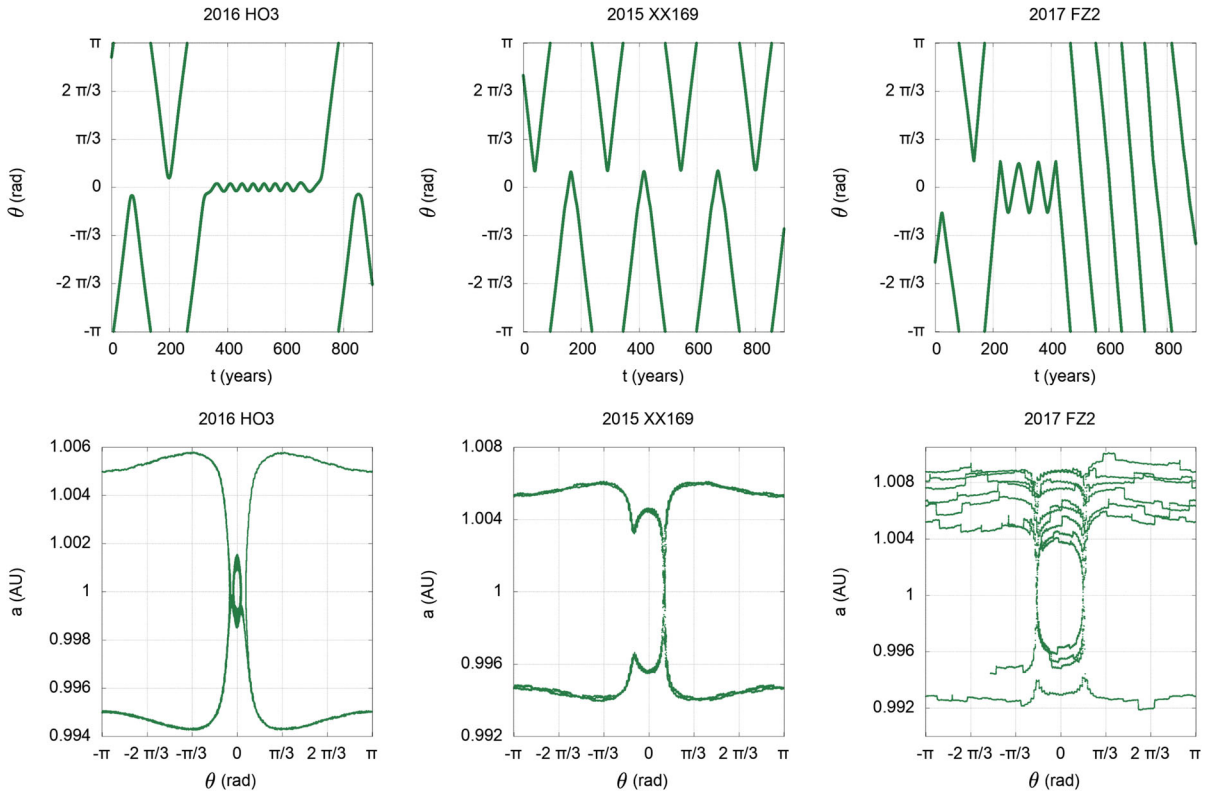

Fig. 5 Coexistence of different regimes. Left: transition between HS and QS motions; middle: CP motion; right: transitions involving HS, QS and non-resonant regimes. In the upper panels the evolution of the resonant angle θ versus time t is plotted and in the lower panels the semi-major axis a versus θ is represented for three real asteroids in co-orbital motion with the Earth

from HS to QS to again HS is shown. In the middle panels, a CP regime can be appreciated; finally, in the right panels, the asteroid is first in a HS regime, then in a QS orbit and, then, is not more trapped in the resonance, showing a NR regime.

Transitions can be thus characterized by the behavior of the resonant angle in terms of averaged value, but also considering the following.

- The period of oscillation of the resonant angle θ changes consistently according to the given co-orbital regime [5,25,28,38,44,48]. This is important to define the time windows to apply the SJM method.
- The time derivative of the resonant angle θ depends on the mean motion n of the asteroid by means of the Lagrange planetary equations [27], and thus its variation is strictly related to a transition.
- The amplitude of the oscillations of the TP, HS, QS motions depends strongly on the eccentricity of the orbit of the asteroid [36].
- At the transition from HS to QS and from QS to HS, the argument of the pericenter ω_r is a stationary point [5,28]. See Fig. 6.
- The relative eccentricity e_r and inclination i_r can provide conditions about the possibility to be in a particular co-orbital state. For example, the condition $i < e_r$ is necessary to get a stable QS phase [48].

Finally, in [17,36], thanks to the identification of the fast and slow variables of the Hamiltonian system assuming a planar[4] approximation of the CR3BP, we have shown that the averaged approximation of the dynamics is able to classify the three co-orbital regimes

[4] i.e., the asteroid orbits the Sun on the same orbital plane of the planet.

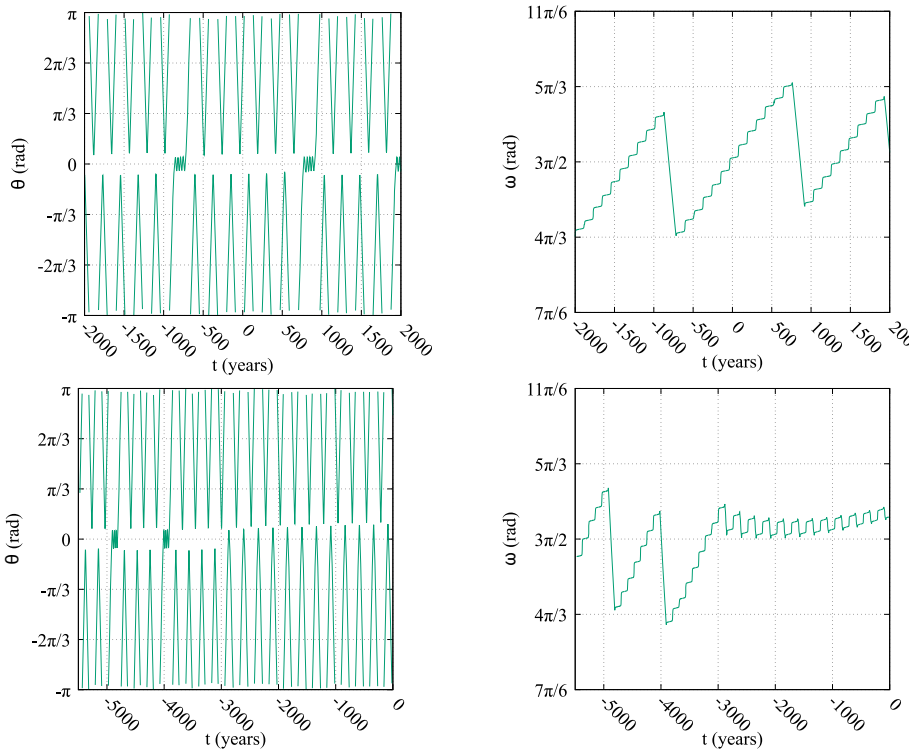

Fig. 6 Orbital evolution of θ (left) and ω (right) for the asteroids 2015 SO2 (top—transition between HS and QS) and 2015 XX169 (bottom—transition between HS and QS plus a CP motion). When ω decreases we have a QS regime; during the CP motion the behavior is the composition of the QS and the HS regimes

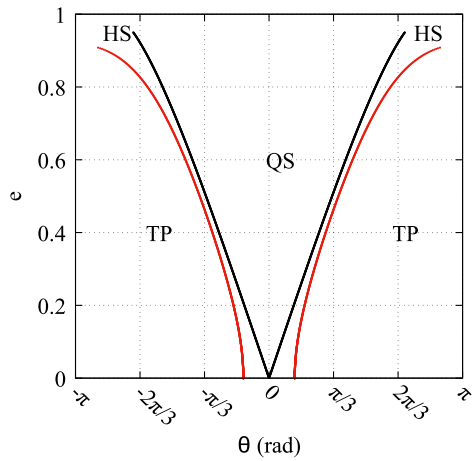

Fig. 7 The (θ, e) map. According to the value of θ and e of the orbit of the particle at the intersection between the semi-major axis of the particle with the one of the planet, we can classify the co-orbital state in the planar approximation. The black curve corresponds to the collision with the planet, the HS motion takes place between the black and the red curve. Inside the black curves, we have the QS domain; outside the red curves we have the TP domains

above in terms of the value that the variables θ and e take when the value of semi-major axis of the particle is equal to the one of the planet. This is what we call the (θ, e) map, that is shown in Fig. 7.

3 Data

The following analysis focuses on the dynamical evolution of particles coming from two different sources. In the first case, the maximum time span is relatively short and the dynamics quite regular. In the second case, the co-orbital motion can persist much longer and can present a complex and rich variety of transitions, also including non-resonant states. This is the testbed for the data that planetary scientists usually handle. We have:

- *dataset 1:* real asteroids in co-orbital motion with the Earth. The given asteroid is found by means of the procedure described in [17], that is, summarizing, by retrieving from the JPL Horizons system [29,30] the ephemerides of asteroids that at the date

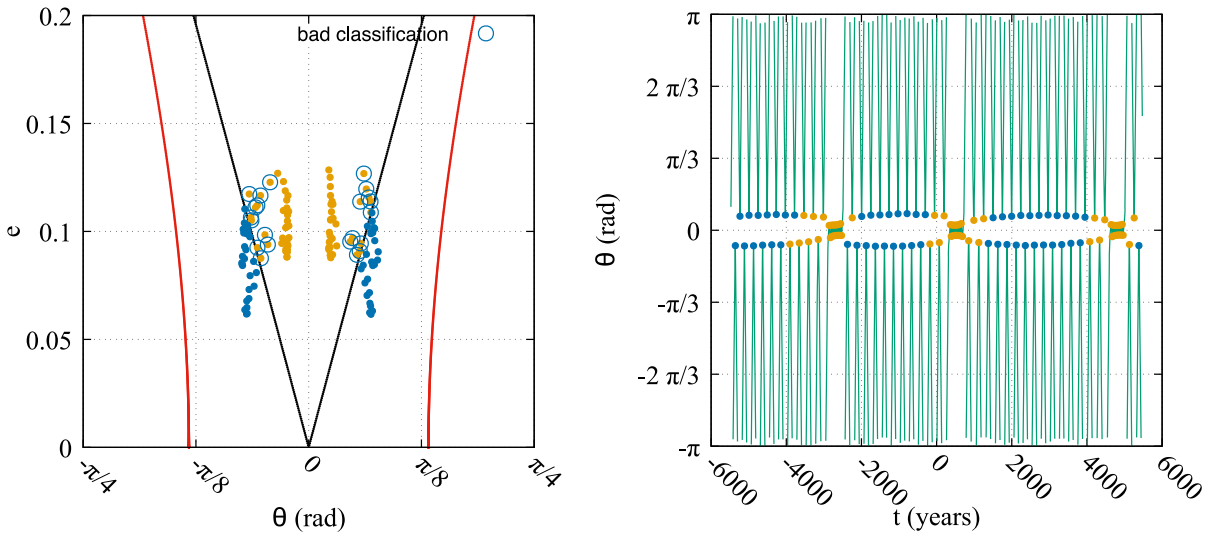

Fig. 8 Left: classification of the co-orbital motion of the asteroid 2016 HO3, according to the (θ, e) map. In orange the points classified as quasi-satellite, the blue circle points are those that are not quasi-satellite in reality, the blue dots are those that are horseshoe and are classified properly. The black curves define the boundary of the quasi-satellite regime, while the red ones the ones of the tadpole motion, between them we have the horseshoe motion. Right: the time evolution of θ and the points used for the classification

March 31, 2021 00:00 have a heliocentric semi-major axis in the range $a \in [0.971, 1.029]$ AU and looking whether and how long a crosses the value 1 AU. If it happens at least once in the whole time frame available from the system (up to 900 years), then the asteroid is a co-orbital candidate. In this way, we have selected 11 asteroids, that exhibit a QS, a HS, a CP behavior or transitions between these regimes[5]. The given ephemerides have been then extended by means of the REBOUND software [40] forward and backward in time to find the maximum interval where the co-orbital motion is seen (some thousands of years, depending on the specific case). The model accounts for the gravitational attraction of Sun, Moon and all the planets, and the ephemerides are generated at a time step of 1000 days. The selected asteroids are: 2001 GO2, 2004 GU9, 2019 GM1, 2016 CA138, 2002 AA29, 2015 SO2, 2015 XX169, 2016 CO246, 2020 PN1, 2020 PP1, 2016 HO3. Given the low number of cases and the relatively short time frame, it has been possible to label, by visual inspection, all the intervals of the corresponding time series according to the co-orbital regime they exhibit.

The identification we aim to achieve through machine learning can, for example, be applied to this kind of data to detect failures in the (θ, e) map, and consequently refine the theory. As an example, in Fig. 8, we show the case of the asteroid Kamo'oalewa (2016 HO3). Each time the semi-major axis crosses $a = 1$ AU, we compute the corresponding values of (θ, e) and evaluate the domain they belong to. Recalll that the domains are defined by the curves depicted in Fig. 7. It appears that the points close to the boundary between the QS and the HS regimes (black lines on the left plot) are not evaluated correctly as HS. The reason lies likely in the orbital inclination, that oscillates in between 7° and 8°, and thus the assumption of co-planarity might not hold. The map can also fail when additional effects, e.g., a fourth body, play a significant role in shaping the dynamics. This is not the case for this specific example, but can happen for instance if the eccentricity is high enough to cross the orbit of Venus.

- *dataset 2:* simulated lunar ejecta, that were generated for the work [20]. The underlying idea is

[5] For this dataset, we do not have transitions involving TP regimes, because we are considering asteroids in co-orbital motion with the Earth and thus we have not found them.

that there occurred a high energetic impact in the past that was able to generate fragments that left the Moon with a launch speed in between the lunar escape velocity and 5.4 km/s. These particles have been propagated for millions of years at a time step of 7500 days to measure how many can be temporarily captured by the Earth and how long. This is not of interest here, but during the non-capture phase many particles can exhibit a co-orbital feature well outside the Earth's Hill sphere and can be used for our purpose. In this case, the data are much more complex than before, given the much longer time frame. They needed an additional pre-filtering to consider only the intervals of time that can contain resonant motions. This is done following [17], that is, removing the intervals where the heliocentric semi-major axis is outside the range specified above, namely, $a \in [0.971, 1.029]$ AU. The whole dataset comprises 7657 time series of different time length. It is beyond the scope of this work to analyze the whole set of data, but it is important to notice that given the high number of cases, the length and the multiple regimes, it has not been possible to label the time intervals as in *dataset 1*. In what follows, we consider only few cases to develop the method. Once defined, it it will serve to extract important statistics over all the trajectories of the dataset.

4 Statistical sparse jump model

We now analyze the time series as described above using the statistical SJM, which is an unsupervised machine learning method designed to identify underlying states (or regimes) within a system by analyzing observed features and their temporal evolution. It assumes that the system's dynamics is governed by an unobserved discrete latent process, which transitions between states over time. The model takes as input a data matrix with T rows (representing epochs), each denoted as $\boldsymbol{y}_t \in \mathbb{R}^P$, and P columns (representing features). Each row $\boldsymbol{y}_t$ corresponds to a snapshot of the system at a specific time t, while features are distinct characteristics or measurements of the system, including orbital elements such as a, e, ω, and θ, as well as summary statistics derived from these elements (e.g., their mean or variance over a specific time window). These features provide a comprehensive representation of the system's state and its underlying dynamics. The model produces three main outputs:

1. A sequence of latent states $\boldsymbol{s} = (s_1, \ldots, s_T)'$, where each s_t takes a value from the discrete set $\{1, 2, \ldots, K\}$ (e.g., QS, HS, etc., corresponding to distinct co-orbital regimes in our context). This sequence provides the inferred regime for each time step based on the observed data and the underlying dynamics.
2. A series of vectors of state-conditional means $\boldsymbol{\mu} = \{\boldsymbol{\mu}_1, \ldots, \boldsymbol{\mu}_K\}$, where each $\boldsymbol{\mu}_k \in \mathbb{R}^P$ represents the average feature values within a given state k. These vectors summarize the characteristics of each regime.
3. A vector of feature importance weights $\boldsymbol{w} = (w_1, \ldots, w_P)$, where each weight w_p quantifies the relevance of the corresponding feature in explaining the system's dynamics. This provides insights into which features are most influential in identifying the regimes.

The model is estimated by solving the following optimization problem

$$\begin{array}{ll} \max_{s_1,\ldots,s_T,\boldsymbol{\mu},\boldsymbol{w}} & \boldsymbol{w}' \sum_{k=1}^{K} n_k \left(\boldsymbol{\mu}_k - \overline{\boldsymbol{\mu}}\right)^2 - \lambda \sum_{t=1}^{T-1} \mathbb{I}(s_t \neq s_{t+1}), \\ \text{subject to} & \|\boldsymbol{w}\|^2 \leq 1, \quad \|\boldsymbol{w}\|_1 \leq \kappa, \\ & w_i \geq 0, \quad \forall i = 1, \ldots, P, \end{array} \tag{5}$$

where n_k denotes the number of time points assigned to state k ($k = 1, \ldots, K$), that is, the count of observations (rows in the input matrix) for which the latent state s_t equals k. This value represents how frequently state k is inferred during the analysis; $\overline{\boldsymbol{\mu}} \in \mathbb{R}^P$ represents the unconditional mean vector of the features (averaged across all states).

The term $\mathbb{I}(s_t \neq s_{t+1})$ counts the number of transitions between states, representing a penalty term that discourages frequent switching between states. The hyperparameter[6] $\lambda \geq 0$ determines the strength of this penalty. A higher λ value increases the penalty for state changes, resulting in smoother transitions and longer durations within individual states. Conversely, when $\lambda = 0$, the model behaves like a k-means algorithm, where no penalty is applied, and state assignments are based solely on clustering the features.

[6] Hyperparameters are parameters whose values are set before training the model and are not learned from the data.

The other hyperparameter, $1 \leq \kappa \leq \sqrt{P}$, controls the sparsity of the feature weights. A lower κ leads to fewer features being selected (e.g., $\kappa = 1$ assigns full importance to a single feature), while a higher κ allows for a more distributed importance across features (e.g., $\kappa = \sqrt{P}$ distributes importance evenly). The constraints on κ ensure that some feature weights are set to zero and that the remaining weights sum to one.

In [33], the authors show that the optimization problem defined in Eq. (5) can be effectively solved through an iterative process that alternates three steps: (a) fitting the model parameters given the current state sequence $\boldsymbol{s}$ and weights $\boldsymbol{w}$, (b) determining the state sequence $\boldsymbol{s}$ by solving a dynamic programming problem, and (c) updating the weights $\boldsymbol{w}$ using a soft thresholding method. Estimation is fast and efficient, typically within only a few iterations, making these models suitable for real-time applications involving considerable amount of data. We refer the reader to [33] for further details on the estimation algorithm.

In the following, we apply the SJM to a set of features derived from orbital elements. The resulting state sequence $\boldsymbol{s}$ represents the sequence of co-orbital regimes, each linked to a distinct state-conditional mean vector $\boldsymbol{\mu}_k$, $k = 1, \ldots, K$, that enables to infer valuable insights for characterizing each orbital regime. Additionally, each feature is given with a weight w_p, $p = 1, \ldots, P$, reflecting its significance in driving the dynamics of the asteroid.

The selection of hyperparameters in SJMs is typically done by using the *generalized information criterion* (GIC) [10,11], which balances model complexity and goodness-of-fit to avoid overfitting. The model selection process involves setting a grid of reasonable values for the hyperparameters, estimating an SJM for each pair, and then choosing the model with the lowest GIC. While the GIC has demonstrated high efficiency in both simulation studies and financial applications, we have observed that it may occasionally overestimate the number of regimes K in this context. To address this, we adopt a heuristic approach: λ and κ are selected based on the GIC, while K is determined a priori through simple exploratory analysis, such as examining time series plots of θ or a. This balance between data-driven selection and a priori information enhances both the practical relevance and interpretability of the model.

All **R** [39] functions for estimating SJM and computing GIC, along with a usage example on a toy dataset, are available on the first author's GitHub page.[7] Estimation is highly efficient, as it requires only a few minutes even for time series with a considerable number of observations.

4.1 Two-regime cases

We start by focusing on the identification of the co-orbital regimes for two cases belonging to *dataset 1*, specifically 2002 AA29 and 2016 HO3[8] (see Sect. 3).

As mentioned before, the dynamics of θ plays a key role in classifying the transitions between co-orbital motions. For this reason, we fit a SJM using features based solely on θ, given its superior predictive capability for co-orbital dynamics. Specifically, we utilize θ and its first differences, denoted as $d\theta$. As suggested by [12,34], volatility (a measure of variability or fluctuations in a time series over a given period) is crucial for tracking regimes as it helps capture periods of dynamic change and identify transitions between different states. To measure volatility, we include moving standard deviations of θ and $d\theta$, denoted as $\sigma_l(\theta)$ and $\sigma_l(d\theta)$. We compute these two latter features by sliding a window of size l over the data and calculating the standard deviation at each step using only the data points within the current window. Here, we use[9] $l = 10$, which is consistent with the libration period of the resonant angle of the two asteroids considered, namely, 2002 AA29 and 2016 HO3. As a matter of fact, the $l = 10$ steps corresponds to about 25 years; the QS libration period of the asteroid 2002 AA29 is about 15 years, while the HS libration period lasts about 190 years ([5,48]) and the QS libration period of the asteroid 2016 HO3 is about 40 years, while its HS libration period is about 260 years. So a shorter window can well

[7] https://github.com/FedericoCortese/GIC-for-SJM/tree/main.

[8] Results on regime identification for other asteroids are available upon request.

[9] We initially tested two window sizes, $l = 10$ (about 25 years) and $l = 75$ (about 200 years), but the model consistently favors the smaller window, as it better captures local fluctuations and transient dynamics. We highlight that selecting an inappropriate window size, however, could lead to suboptimal performance, either by missing important variations or introducing noise. Based on our experience, carefully choosing l a priori remains critical, and further research into its automated selection is planned.

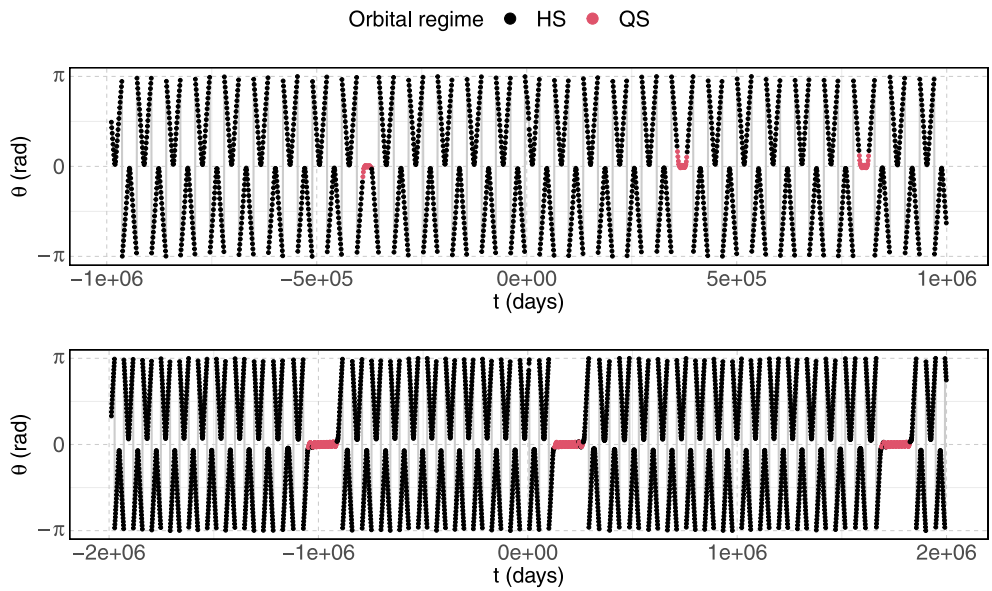

Fig. 9 Regime identification for 2002 AA29 (top) and 2016 HO3 (bottom), with black dots indicating the horseshoe (HS) regime and red dots indicating the quasi-satellite (QS) regime

highlight the different features between the QS and a HS regimes, while a longest window would lose such features.

The final datasets comprise $T = 1\,989$ and $T = 3\,988$ observations, respectively, with each time step corresponding to 1 000 days, and a total of $P = 4$ features per dataset, specifically θ, $d\theta$, $\sigma_l(\theta)$ and $\sigma_l(d\theta)$.

As these data were labeled, as explained in Sect. 3, we evaluate the performance of the model using the balanced accuracy (BAC) computed between true and estimated state sequences. BAC is defined as

$$\text{BAC} = \frac{1}{K}\sum_{k=1}^{K}\frac{tp_k}{tp_k + fn_k},$$

where tp_k and fn_k denote the number of true positives and false negatives, respectively, for the state k. The model achieves exceptional accuracy, with a BAC of 99% for both asteroids 2002 AA29 and 2016 HO3. Figure 9 illustrates the time evolution of θ for 2002 AA29 (top) and 2016 HO3 (bottom). Each dot in the figure represents a single time step, and it is colored black for the HS regime and red for the QS regime, as estimated by the SJM.[10]

Out of the original four features, two are identified as relevant: the moving standard deviations of θ and $d\theta$. These features account for around 76% and 23% of the total feature weights across both asteroids, respectively. Recalling that the time derivative of the resonant angle θ is related to the mean motion n of the asteroid (see Sect. 2), this result highlights the importance of the variation of θ and n to discern the QS regime from the HS one.

The time allocation across co-orbital regimes reveals comparable patterns in the two cases: 2002 AA29 spends 96.63% of its time in the HS regime and 3.37% in the QS regime, with average durations of 480 150 days (about 1 315 years) and 22 330 days (about 61 years), respectively. Similarly, 2016 HO3 spends 90.05% of its time in the HS regime and 9.95% in the QS regime, with average durations of 399 000 days (about 1 093 years) and 49 625 days (about 136 years).

Table 1 present the state-specific means and standard deviations for θ, e, and ω. While we do not include features related to ω and e in the SJM estimation process, we report them here to illustrate their behavior across regimes. Specifically, the volatility of θ remains the primary distinguishing factor, being 5 to 20 times higher in the HS regime compared to the QS regime. In contrast, ω shows differences between regimes for 2002 AA29 but remains consistent for 2016 HO3, whereas e differs across regimes for 2016 HO3 but is consistent across regimes for 2002 AA29. These similarities reduce the

[10] The GIC selects $\lambda = 0$ and $\kappa = 1.25$ for both datasets.

Table 1 Mean and standard deviation (σ) of orbital elements for horseshoe (HS) and quasi-satellite (QS) regimes of asteroids 2002 AA29 and 2016 HO3

Variable	2002 AA29		2016 HO3	
	HS	QS	HS	QS
θ	3.138	0.033	3.140	0.000
$\sigma(\theta)$	1.798	0.128	1.836	0.056
e	0.028	0.045	0.093	0.104
$\sigma(e)$	0.016	0.012	0.017	0.012
ω	1.936	0.961	4.815	4.717
$\sigma(\omega)$	1.629	0.530	0.720	0.602

ability of ω and e to discriminate between regimes, potentially introducing confounding effects. Tests conducted with SJMs incorporating ω- and e-related features consistently yielded worse performance, further supporting their exclusion from the final model.

4.2 Complex cases

In this section, we examine more complex scenarios where an asteroid can experience transitions between multiple regimes. We focus on two time series as from the *dataset 2* described in Sect. 3. For these cases, the features used in the previous section are enriched to catch all the possible situations, in particular the NR and the CP cases.

Specifically, the NR regimes can be identified by analyzing the oscillation in semi-major axis a (which never crosses the value of the semi-major axis of the planet). Therefore, we include a as a feature and the indicator variable $\mathbb{I}(a)_t = \mathbb{I}(a_{t:(t-l+1)} > 1 \vee a_{t:(t-l+1)} < 1)$, which tracks whether, at each time step t, all of the previous l observations[11] $a_{t:(t-l+1)}$ are either above or below 1. We denote the resulting feature as $\mathbb{I}(a)$. Moreover, the volatility of the CP motion can be very close to the one of HS regime, and also the mean of the CP motion is not well defined, being a combination of HS and QS. Based on these considerations, to capture the specific characteristics of the resonant regimes and to quantify oscillation differences, we first identify the local maxima and minima of θ using the `peaks` function or the **splus2R** package in `R`. Based on these extrema, we then construct the following additional features:

- For each time step t, we define $\max(\theta)_t$ and $\min(\theta)_t$ as the last observed maximum and minimum values of θ, respectively. Using these, we compute the following features:
  - $\mathbb{I}(\text{TP})_t = \mathbb{I}\big(\max(\theta)_t \cdot \min(\theta)_t > 0 \wedge \max(\theta)_t > \min(\theta)_t\big)$
  - $\mathbb{I}(\text{QS})_t = \mathbb{I}\big(\max(\theta)_t \cdot \min(\theta)_t < 0 \wedge \max(\theta)_t > \min(\theta)_t\big)$
  - $\mathbb{I}(\text{HS})_t = \mathbb{I}\big(\max(\theta)_t \cdot \min(\theta)_t < 0 \wedge \max(\theta)_t < \min(\theta)_t\big)$
  - $\mathbb{I}(\text{CP})_t = \mathbb{I}\big(\max(\theta)_t \cdot \min(\theta)_t > 0 \wedge \max(\theta)_t < \min(\theta)_t\big)$
- Additionally, we compute the mean oscillation Θ_t as

$$\Theta_t = \mathbb{I}(\text{HS})_t \cdot \frac{\min(\theta)_t + \max(\theta)_t + 2\pi}{2} + \{\mathbb{I}(\text{QS})_t + \mathbb{I}(\text{TP})_t\} \cdot \frac{\min(\theta)_t + \max(\theta)_t}{2}.$$

We denote the resulting features as $\mathbb{I}(\text{TP})$, $\mathbb{I}(\text{QS})$, $\mathbb{I}(\text{HS})$, $\mathbb{I}(\text{CP})$, and Θ, respectively. In the absence of labeled data, we evaluate the results through qualitative assessment, emphasizing interpretability and consistency with theoretical expectations. The final datasets consist of $T = 4\,917$ and $T = 6\,653$ observations each. The number of features is $P = 11$ in both cases.

For these complex cases, where ground truth labels are not available, classification accuracy is evaluated qualitatively. This involves visually inspecting the resulting graphs and assessing the consistency of the identified regimes with the expected co-orbital dynamics.

Example 1

A preliminary analysis identifies four regimes in this case: HS, QS, CP, and NR phases. Figure 10 shows the regime identification with a and θ over a zoomed-in time frame, highlighting the behavior of each regime as estimated by the SJM,[12] with different colors. The method is particularly effective in identifying NR and QS regimes, except for some time steps where the regime is identified with a slight delay. HS is also clearly identified, although it is occasionally misclassified as CP.

The asteroid spends 12.77%, 63.96%, 13.14%, and 10.13% of the time in the regimes NR, HS, QS, and

[11] As in previous cases, we set $l = 10$.

[12] In this case, the GIC selects $\lambda = 15$ and $\kappa = 2.5$.

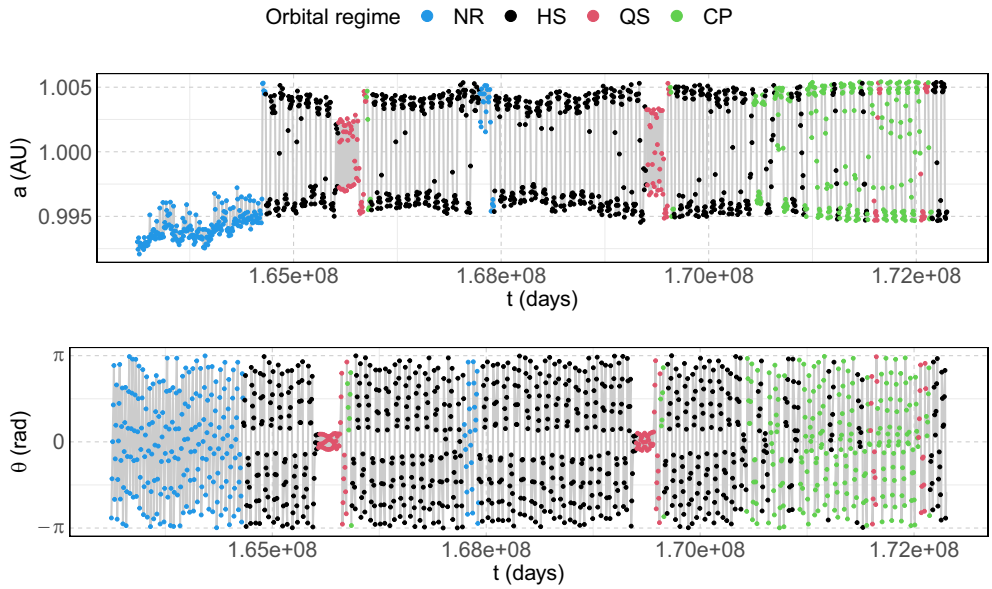

Fig. 10 Regime identification for Example 1, displaying a (top) and θ (bottom). Dots colors indicate different regimes: black for horseshoe (HS), red for quasi-satellite (QS), blue for non-resonant (NR), green for compound (CP). The time frame on these two panels focuses on a shorter period compared to the whole time span of propagation

CP, respectively, with an average duration of 2 355 000, 673 929, 161 500, and 133 393 days (which corresponds to approximately 6452, 1846, 442, and 365 years, respectively). Table 2 presents the mean and standard deviations of θ, e, ω, and a, conditioned on the regime classification.

The results confirm the importance of the volatility of θ in identifying the QS regime, as it is lower with respect to other regimes. We observe no significant differences in e or its volatility. The semi-major axis a remains close to 1 on average, except in the NR regime, as expected, further supporting the meaningfulness of the state classification.

Table 3 shows the weights of the selected features. The indicator $\mathbb{I}(a)$ holds the highest weight (0.223), highlighting its key role in distinguishing regimes, particularly as a discriminant for the NR phase. $\mathbb{I}$(CP) and $\mathbb{I}$(QS) follow, each with a weight of approximately 0.18, aiding in tracking the QS and CP phases. Additionally, the volatility of θ confirms its importance in differentiating orbital phases.

Example 2

In this case, exploratory analysis suggests the presence of five regimes: NR, HS, QS, CP, and TP. Figure 11 illustrates the regime identification,[13] showing the semi-major axis a and angle θ over a zoomed-in time window. We mark regimes in black (HS), red (QS), blue (NR), green (CP), and violet (TP). The method identifies NR and QS effectively, though TP occasionally overlaps with HS, and some NR points are misclassified as CP.

Table 2 Mean and standard deviation (σ) of orbital elements θ, e, ω, and a for asteroid of Example 1 for non-resonant (NR), horseshoe (HS), quasi-satellite (QS), and compound (CP) regimes

Feature	NR	HS	QS	CP
θ	−0.008	3.138	−0.108	3.272
$\sigma(\theta)$	1.812	1.842	1.345	1.759
e	0.198	0.129	0.132	0.156
$\sigma(e)$	0.007	0.036	0.028	0.026
ω	1.884	4.414	4.210	4.236
$\sigma(\omega)$	0.698	1.183	0.764	0.809
a	0.987	1.000	1.000	1.000
$\sigma(a)$	0.008	0.005	0.004	0.005

[13] In this latter case, the GIC selects $\lambda = 10$ and $\kappa = 3$.

Table 3 Selected features and their corresponding weights for Example 1

Feature	Weight
$\mathbb{I}(a)$	0.223
$\mathbb{I}$(QS)	0.187
$\mathbb{I}$(CP)	0.182
$\sigma_l(d\theta)$	0.158
$\sigma_l(\theta)$	0.090
a	0.060
$\mathbb{I}$(HS)	0.060
Θ	0.040

The asteroid spends 19.00%, 16.40%, 1.80%, 5.67%, and 57.16% of the time in regimes NR, HS, QS, CP, and TP, respectively. The average times (in days) spent in each regime are 3 160 000, 1 168 929, 442 500, 235 625, and 3 565 313 days in NR, HS, QS, CP, and TP, respectively (corresponding to approximately 8 658, 3 203, 1 212, 648, and 9 769 years).

Table 4 summarizes the mean and standard deviations of θ, e, ω, and a across the five regimes. QS consistently exhibits lower volatility in θ, while e and its volatility show no significant differences. The semi-major axis a deviates from being centered at 1 in the NR regime, as expected. Although ω appears to differentiate between regimes, this was not observed in the previous example, indicating that its role in regime classification may be context-dependent or influenced by specific characteristics of the analyzed dataset.

Table 5 reports the selected variables and their corresponding weights. $\mathbb{I}$(HS), $\mathbb{I}$(CP), $\mathbb{I}$(TP), and $\mathbb{I}$(QS) have similar and high weights. The mean oscillation Θ has a weight of 0.117. The standard deviations of θ and $d\theta$ are also key contributors, with weights of 0.112 and 0.113, respectively. Finally, the indicator $\mathbb{I}(a > 1)$, with a weight of 0.098, remains a critical feature for identifying transitions, particularly in distinguishing the NR regime.

5 Discussion

The SJM has demonstrated exceptional performance in simple scenarios, providing accurate and efficient classification. In more complex cases, where preliminary manual labeling for accuracy assessment would be cumbersome, the method still achieves qualitatively strong results, significantly reducing the need for human intervention in co-orbital regime identification.

Our results are consistent with theoretical expectations, enhancing their applicability and interpretability. In fact, the analysis confirms that θ is the primary

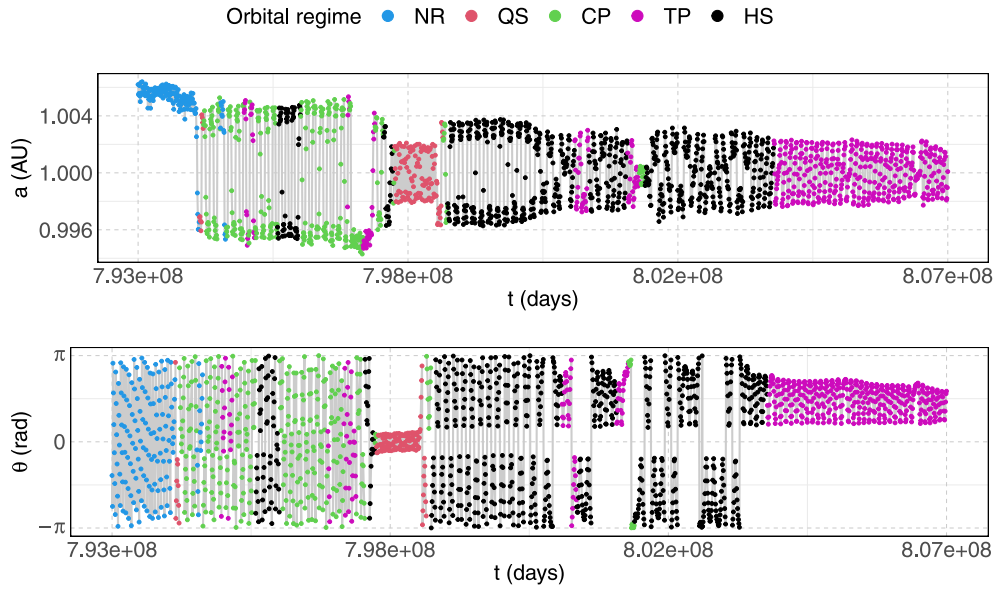

Fig. 11 Regime identification for Example 2, displaying a (top) and θ (bottom). Dots colors indicate different regimes: black for horseshoe (HS), red for quasi-satellite (QS), blue for non-resonant (NR), green for compound (CP), and violet for tadpole (TP)

Table 4 Mean and standard deviation (σ) of θ, e, ω, and a for asteroid of Example 2 for non-resonant (NR), horseshoe (HS), quasi-satellite (QS), compound (CP), and tadpole (TP) regimes

Feature	NR	HS	QS	CP	TP
θ	0.033	3.196	− 0.178	3.221	1.297
$\sigma(\theta)$	1.813	2.040	0.899	1.871	0.538
e	0.221	0.226	0.237	0.197	0.215
$\sigma(e)$	0.014	0.021	0.013	0.019	0.018
ω	2.894	2.282	1.459	1.716	3.328
$\sigma(\omega)$	1.674	1.076	0.337	0.504	1.874
a	1.008	1.000	1.000	1.000	1.000
$\sigma(a)$	0.004	0.003	0.002	0.004	0.001

Table 5 Selected variables and their corresponding weights for asteroid of Example 2

Feature	Weight
$\mathbb{I}$(HS)	0.127
$\mathbb{I}$(CP)	0.127
$\mathbb{I}$(TP)	0.123
$\mathbb{I}$(QS)	0.122
Θ	0.117
$\sigma_l(d\theta)$	0.110
$\sigma_l(\theta)$	0.101
$\mathbb{I}(a)$	0.100
a	0.064
θ	0.016

driver distinguishing different phases, with a playing a critical role in the occurrence of NR regime. Additionally, the method enables straightforward extraction of key dynamical metrics, such as the average duration of regimes and the transitions between them. Applying this method to a sufficiently large sample of objects will allow for a more precise characterization of the co-orbital behavior. In the long term the procedure introduced can be considered to analyze also different kinds of dynamics. The first natural extension would be the identification of transitions between mean motion resonance of various order, i.e., not only within the co-orbital motion. In addition, since the method provides well-defined metrics on selected features, i.e., variables, it would be possible to use this information also in the field of asteroid family members identification [32], for instance by using these metrics to look for given clusters.

While the method demonstrates high accuracy and interpretability, some aspects suggest that further discussion and improvements are needed. One of the primary challenges lies in hyperparameter tuning, which can influence the performance of the model. A potential solution to address the issue of selecting K (the number of regimes) a priori is to employ Bayesian nonparametric methods, where K is inferred directly from the data [19]. That said, it is important to note that our analysis relies on extensive preliminary work on the data: future applications will benefit from this effort without needing repeated parameter tuning or initial feature screening.

The choice of window length, determined through visual inspection for certain feature computations such as moving volatility, represents another important aspect with room for further improvements. The choice made in this work reflects a synergy among the SJM, our understanding of celestial mechanics and the specific dynamics of the problem. In particular, the method should be able to catch the period of the QS regime, that is theoretically the shortest one among the various regimes, but it is also constrained by the number of observations in the chosen window. It has to be considered also the objective of the application: for the cases shown here the ephemerides of the simpler cases have a finer time step to detect very short regimes switching, while the ephemerides of the complex cases were generated to compute a statistical estimate of the overall behavior.[14] Notice that the method has been proved also in the complex scenarios with a relatively large time step.[15] Whenever possible, its effectiveness would improve with finer temporal resolutions.

To address these limitations, several potential developments are worth exploring. One promising approach is the introduction of regime-dependent feature weights, which could enhance the model's adaptability by better capturing the unique dynamics of each co-orbital regime. This refinement would not only improve the model's precision but also increase its interpretability, particularly in more complex scenarios. For instance, theoretical insights indicate that significant changes in the semi-major axis a occur predominantly in the NR case. However, the current SJM framework assigns fea-

[14] That will be the objective of the next work.

[15] Notably, for simulations spanning millions of years, a time step of 7500 days is already a significant advantage.

ture importance uniformly across all regimes, without distinguishing between them.

Another potential improvement is integrating physics insights directly into the SJM framework using the so-called physics-informed machine learning approach [22]. By embedding known dynamical relationships, the model could enhance its predictive accuracy and generalization.

Author contributions F.C. developed the method and analyzed the results. S.D.R. contributed to Sect. 2 and to refine the feature selection and the results interpretation. E.M.A. conceived the study, generated the data and contributed to refine the feature selections and the results interpretation. All authors reviewed the manuscript.

Funding Open access funding provided by Consiglio Nazionale Delle Ricerche (CNR) within the CRUI-CARE Agreement. The authors have not disclosed any funding.

Data availability The numerical data sets generated and analyzed during the current study are available from the corresponding author upon reasonable request.

Declarations

Conflict of interest The authors declare no competing interests.

References

1. Akioka, M., Nagatsuma, T., Miyake, W., Ohtaka, K., Marubashi, K.: The L5 mission for space weather forecasting. Adv. Space Res. **35**(1), 65–69 (2005)
2. Aydınhan, A.O., Kolm, P.N., Mulvey, J.M., Shu, Y.: Identifying patterns in financial markets: extending the statistical jump model for regime identification. Ann. Oper. Res. (2024). https://doi.org/10.1007/s10479-024-06035-z
3. Bartolucci, F., Farcomeni, A., Pennoni, F.: Latent Markov Models for Longitudinal Data. Chapman & Hall/CRC Press (2013)
4. Bemporad, A., Breschi, V., Piga, D., Boyd, S.P.: Fitting jump models. Automatica **96**, 11–21 (2018)
5. Brasser, R., Innanen, K., Connors, M., Veillet, C., Wiegert, P., Mikkola, S., Chodas, P.: Transient co-orbital asteroids. Icarus **171**(1), 102–109 (2004)
6. Caritá, G., Aljbaae, S., Morais, M., Signor, A., Carruba, V., Prado, A., Hussmann, H.: Image classification of retrograde resonance in the planar circular restricted three-body problem. Celest. Mech. Dyn. Astron. **136**(2), 10 (2024)
7. Carruba, V., Aljbaae, S., Domingos, R.C., Huaman, M., Barletta, W.: Machine learning applied to asteroid dynamics. Celest. Mech. Dyn. Astron. **36**, 134 (2022)
8. Carruba, V., Aljbaae, S., Smirnov, E., Caritá, G.: Vision transformers for identifying asteroids interacting with secular resonances. Icarus **425**, 116346 (2025)
9. Ciacci, G., Barucci, A., Di Ruzza, S., Alessi, E.M.: Asteroids co-orbital motion classification based on machine learning. Mon. Not. R. Astron. Soc. **527**(3), 6439–6454 (2024)
10. Cortese, F. P., Kolm, P. N., Lindstrom, E.: Generalized information criteria for high-dimensional sparse statistical jump models. Available at SSRN 4774429 (2024)
11. Cortese, F.P., Kolm, P.N., Lindström, E.: Generalized information criteria for sparse statistical jump models. Symposium i Anvendt Statistik **44**, 68–78 (2023)
12. Cortese, F. P., Kolm, P. N., Lindström, E.: What drives cryptocurrency returns? A sparse statistical jump model approach. Digital Finance, pp 1–36 (2023)
13. Cortese, F. P., Pievatolo, A.: Spatio-temporal jump model for urban thermal comfort monitoring. arXiv preprint arXiv:2411.09726 (2024)
14. Cortese, F. P., Pievatolo, A.: Statistical jump model for mixed-type data with missing data imputation. Advances in Data Analysis and Classification, pp 1-25 (2025)
15. de la Fuente Marcos, C., de la Fuente Marcos, R.: On the dynamical evolution of 2002 VE68. Monthly Not. R. Astron. Soc. **427**(1), 728–739 (2012)
16. de la Fuente Marcos, C., de la Fuente Marcos, R.: Asteroid (469219) 2016 HO3, the smallest and closest Earth quasi-satellite. Monthly Not. R. Astron. Soc. **462**(4), 3441–3456 (2016)
17. Di Ruzza, S., Pousse, A., Alessi, E.M.: On the co-orbital asteroids in the solar system: medium-term timescale analysis of the quasi-coplanar objects. Icarus **390**, 115330 (2023)
18. Eckman, R. A., Barrett, C., Batcha, A. L., Killeen, B. J.: Trajectory operations of the Artemis I mission. In 2023 AAS/AIAA Astrodynamics Specialist Conference, Big Sky, MT, (2023). Paper AAS 23-363
19. Giampino, A., Guindani, M., Nipoti, B., Vannucci, M.: Local level dynamic random partition models for changepoint detection. arXiv preprint arXiv:2407.20085 (2024)
20. Jedicke, R., Alessi, E. M., Wiedner, N., Ghosal, M., Bierhaus, E. B., Granvik, M.: The steady state population of Earth's minimoons of lunar provenance. Icarus, in press (2025)
21. Jiao, Y., Cheng, B., Huang, Y., Asphaug, E., Gladman, B., Malhotra, R., Michel, P., Yu, Y., Baoyin, H.: Asteroid Kamo'oalewa's journey from the lunar Giordano Bruno crater to Earth 1:1 resonance. Nat Astron **8**, 819–826 (2024)
22. Karniadakis, G.E., Kevrekidis, I.G., Lu, L., Perdikaris, P., Wang, S., Yang, L.: Physics-informed machine learning. Nat. Rev. Phys. **3**(6), 422–440 (2021)

23. Kawakatsu, Y., Kuramoto, K., Usui, T., Sugahara, H., Ootake, H., Yasumitsu, R., Yoshikawa, K., Mary, S., Grebenstein, M., Sawada, H., Imada, T., Shimada, T., Ogawa, K., Otsuki, M., Baba, M., Fujita, K., Zacny, K., van Dyne, D., Satoh, Y., Tokaji, A.: Preliminary design of Martian Moons eXploration (MMX). Acta Astronaut. **202**, 715–728 (2023)
24. Li, X., Li, J., Xia, Z.J., Georgakarakos, N.: Machine-learning prediction for mean motion resonance behaviour: the planar case. Mon. Not. R. Astron. Soc. **511**(2), 2218–2228 (2022)
25. Mikkola, S., Innanen, K., Wiegert, P., Connors, M., Brasser, R.: Stability limits for the quasi-satellite orbit. Mon. Not. R. Astron. Soc. **369**, 15–24 (2006)
26. Morais, M., Morbidelli, A.: The population of Near-Earth Asteroids in coorbital motion with the Earth. Icarus **160**, 1–9 (2002)
27. Murray, C. D., Dermott, S. F.: Solar system dynamics (1999)
28. Namouni, F.: Secular interactions of coorbiting objects. Icarus **137**(2), 293–314 (1999)
29. NASA. JPL Horizons system. https://ssd-api.jpl.nasa.gov/doc/horizons.htm (2024)
30. NASA JPL SSD small-body database. Small-body database query. https://ssd.jpl.nasa.gov/tools/sbdb_query.html (2024)
31. Norris, J.R.: Markov Chains. Cambridge University Press, D (1997)
32. Novaković, B., Vokrouhlický, D., Spoto, F., Nesvorný, D.: Asteroid families: properties, recent advances, and future opportunities. Celest. Mech. Dyn. Astron. **134**, 34 (2022)
33. Nystrup, P., Kolm, P.N., Lindström, E.: Feature selection in jump models. Expert Syst. Appl. **184**, 115558 (2021)
34. Nystrup, P., Lindström, E., Madsen, H.: Learning hidden markov models with persistent states by penalizing jumps. Expert Syst. Appl. **150**, 113307 (2020)
35. Olkin, C., Vincent, M., Adam, C., Berry, K., Englander, J., Gray, S., Levison, H., Salmon, J., Spencer, J., Stanbridge, D., et al.: Mission design and concept of operations for the Lucy mission. Space Sci. Rev. **220**(4), 47 (2024)
36. Pousse, A., Alessi, E.M.: Revisiting the averaged problem in the case of mean-motion resonances in the restricted three-body problem. Nonlinear Dyn. **108**, 959–985 (2022)
37. Provinciali, L., Bozzoli, L., Saita, G., Amabili, P., Calcagno, D., Pipino, A., Conterio, L., Balossino, A., Alessi, E. M., Cicalò S., Marcucci,, M. F., Laurenza, M., Landi, S., Zimbardo, G.: HEliospheric pioNeer for sOlar and interplanetary threats defeNce (HENON) mission: Space weather monitoring and forecasting. In International Astronautical Congress, (2023). Paper IAC-23,B4,2,2,x79569
38. Qi, Y., Qiao, D.: Co-orbital transition of 2016 HO3. Astrodynamics **7**, 3–14 (2023)
39. R Core Team. R: A Language and Environment for Statistical Computing. R Foundation for Statistical Computing, Vienna, Austria, 2023. Version 4.3.1, accessed December (2024)
40. Rein, H., Liu, S.F.: REBOUND: an open-source multi-purpose N-body code for collisional dynamics. A&A **537**, A128 (2012)
41. Roy, A. E.: Orbital motion (3rd revised and enlarged edition). (1988)
42. Shu, Y., Yu, C., Mulvey, J.M.: Downside risk reduction using regime-switching signals: a statistical jump model approach. J. Asset. Manag. **25**, 493 (2024)
43. Shu, Y., Yu, C., Mulvey, J. M.: Dynamic asset allocation with asset-specific regime forecasts. Ann. Oper. Res. (2024)
44. Sidorenko, V.V., Neishtadt, A.I., Artemyev, A.V., Zelenyi, L.M.: Quasi-satellite orbits in the general context of dynamics in the 1:1 mean motion resonance: perturbative treatment. Celest. Mech. Dyn. Astron. **120**, 131–162 (2014)
45. Smirnov, E.: A new python package for identifying celestial bodies trapped in mean-motion resonances. Astron. Comput. **43**, 100707 (2023)
46. Szebehely, V.: Theory of orbits. Academic Press, The restricted problem of three bodies. New York (1967)
47. Toliou, A., Granvik, M.: Resonant mechanisms that produce near-Sun asteroids. Monthly Noti. R. Astron. Soc. **521**(4), 4819–4837 (2023)
48. Wajer, P.: Dynamical evolution of Earth's quasi-satellites: 2004 GU9 and 2006 FV35. Icarus **209**(2), 488–493 (2010)
49. Williams, J., Dawn, T. F., Batcha, A. L.: A history of Orion mission design, Copernicus software development, and the Artemis I trajectory. In 2023 AAS/AIAA Astrodynamics Specialist Conference, Big Sky, MT, (2023). Paper AAS 23-241
50. Zhang, T., Xu, K., Ding, X.: China's ambitions and challenges for asteroid-comet exploration. Nat. Astron. **5**, 730–731 (2021)
51. Zou, J., Han, Y., So, S.-S.: Overview of artificial neural networks. Artif. Neural Netw. Methods Appl. (2009). https://doi.org/10.1007/978-1-60327-101-1_2
52. Zucchini, W., MacDonald, I.L., Langrock, R.: Hidden Markov Models for Time Series: An Introduction Using r. CRC Press (2017)